

LONDON
SCHOOL of
HYGIENE
& TROPICAL
MEDICINE



Ganter, M; Goldberg, JM; Dvorin, JD; Paulo, JA; King, JG; Tripathi, AK; Paul, AS; Yang, J; Coppens, I; Jiang, RH; Elsworth, B; Baker, DA; Dinglasan, RR; Gygi, SP; Duraisingh, MT (2017) *Plasmodium falciparum* CRK4 directs continuous rounds of DNA replication during schizogony. *Nature microbiology*, 2. p. 17017. ISSN 2058-5276 DOI: <https://doi.org/10.1038/nmicrobiol.2017.17>

Downloaded from: <http://researchonline.lshtm.ac.uk/3515651/>

DOI: [10.1038/nmicrobiol.2017.17](https://doi.org/10.1038/nmicrobiol.2017.17)

Usage Guidelines

Please refer to usage guidelines at <http://researchonline.lshtm.ac.uk/policies.html> or alternatively contact researchonline@lshtm.ac.uk.

Available under license: Copyright the publishers

Plasmodium falciparum CRK4 directs continuous rounds of DNA replication during schizogony

Markus Ganter^{1†}, Jonathan M. Goldberg¹, Jeffrey D. Dvorin^{1,2†}, Joao A. Paulo³, Jonas G. King^{4†}, Abhai K. Tripathi⁴, Aditya S. Paul¹, Jing Yang¹, Isabelle Coppens⁴, Rays H. Y. Jiang^{1†}, Brendan Elsworth¹, David A. Baker⁵, Rhoel R. Dinglasan^{4†}, Steven P. Gygi³ and Manoj T. Duraisingh^{1*}

***Plasmodium* parasites, the causative agents of malaria, have evolved a unique cell division cycle in the clinically relevant asexual blood stage of infection¹. DNA replication commences approximately halfway through the intracellular development following invasion and parasite growth. The schizont stage is associated with multiple rounds of DNA replication and nuclear division without cytokinesis, resulting in a multinucleated cell. Nuclei divide asynchronously through schizogony, with only the final round of DNA replication and segregation being synchronous and coordinated with daughter cell assembly^{2,3}. However, the control mechanisms for this divergent mode of replication are unknown. Here, we show that the *Plasmodium*-specific kinase *PfCRK4* is a key cell-cycle regulator that orchestrates multiple rounds of DNA replication throughout schizogony in *Plasmodium falciparum*. *PfCRK4* depletion led to a complete block in nuclear division and profoundly inhibited DNA replication. Quantitative phosphoproteomic profiling identified a set of *PfCRK4*-regulated phosphoproteins with greatest functional similarity to CDK2 substrates, particularly proteins involved in the origin of replication firing. *PfCRK4* was required for initial and subsequent rounds of DNA replication during schizogony and, in addition, was essential for development in the mosquito vector. Our results identified an essential S-phase promoting factor of the unconventional *P. falciparum* cell cycle. *PfCRK4* is required for both a prolonged period of the intraerythrocytic stage of *Plasmodium* infection, as well as for transmission, revealing a broad window for *PfCRK4*-targeted chemotherapeutics.**

Malaria parasites proliferate through schizogony in the blood stage of infection. A series of rapid rounds of DNA replication and nuclear division produces a syncytial cell with approximately 20 nuclei. In contrast to the synchronous nuclear division observed in other multinucleated cells, such as the early *Drosophila* embryo⁴, *Plasmodium falciparum* nuclei divide asynchronously during the blood stage, despite sharing the same cytoplasm^{2,3}, suggesting that cell-cycle progression is not governed by diffusible cytoplasmic factors. Knockout screens have identified non-essential blood-stage *Plasmodium* kinases and suggested those that could be essential for the regulation of schizogony^{5,6}. The molecular mechanisms

regulating this diverged mode of replication are largely unknown, yet the recent development of conditional gene expression technologies now allows the unequivocal demonstration of gene essentiality in *P. falciparum*^{7–9}.

To directly identify critical regulators of schizogony and simultaneously determine protein function, we adopted the destabilization domain (DD) conditional knockdown approach^{7,10,11}. We generated endogenous DD fusions of 23 schizont-stage kinases in the *P. falciparum* D10 strain and screened for vulnerability to destabilization by DD (Fig. 1a,b and Supplementary Fig. 1a). Using this approach, we found that two kinases, the cGMP-dependent protein kinase (*PfPKG*) and the *cdc2*-related protein kinase 4 (*PfCRK4*), had profound proliferation defects in the absence of Shield-1 and showed dose dependency (Fig. 1c and Supplementary Fig. 1b,c). Chemical inhibition of *PfPKG* has previously established its essential role in parasite egress from erythrocytes at the end of schizogony^{12,13}, now confirmed by conditional destabilization.

As previously observed^{14,15}, we found little correlation between the level of protein knockdown and the ability to reveal the essentiality of other kinases previously thought to be essential⁶ using the DD approach (Fig. 1d and Supplementary Figs 1d and 9). This could be due to insufficient destabilization of these proteins or because they are required at different levels for asexual proliferation.

The biological function of *PfCRK4* is unknown, and we confirmed its essentiality in a different parental line—*P. falciparum* P2G12 (ref. 16)—which also produces gametocytes (Supplementary Fig. 2). *PfCRK4* is a member of an Apicomplexa-specific kinase subfamily related to cyclin-dependent kinases (CDK) (Supplementary Fig. 3 and Supplementary Data 1)^{17,18}. In many organisms, CDKs in complex with cyclins regulate key steps of the cell cycle and other cellular functions^{19,20}. Compared to human CDK2, the kinase domain of *PfCRK4* possesses multiple sequence inserts of unknown function (Fig. 2a and Supplementary Fig. 4).

PfCRK4 is localized to the nucleus of late trophozoites and schizonts, with the signal greatly diminished in segmented schizonts that have undergone cytokinesis (Fig. 2b). Following conditional depletion of *PfCRK4* (Fig. 1d), parasites arrested at the trophozoite-to-schizont transition (Fig. 2c). At ≥ 40 h post invasion (h.p.i.), parasites [+]
Shield-1 (that is, wild-type *PfCRK4* levels)

¹Department of Immunology and Infectious Diseases, Harvard T.H. Chan School of Public Health, 651 Huntington Avenue, FXB, Room 202, Boston, Massachusetts 02115, USA. ²Division of Infectious Diseases, Boston Children's Hospital, Boston, Massachusetts 02115, USA. ³Department of Cell Biology, Harvard Medical School, Boston, Massachusetts 02115, USA. ⁴W. Harry Feinstone Department of Molecular Microbiology & Immunology, The Johns Hopkins Malaria Research Institute, Johns Hopkins Bloomberg School of Public Health, Baltimore, Maryland 21205, USA. ⁵Faculty of Infectious and Tropical Diseases, London School of Hygiene & Tropical Medicine, London WC1E 7HT, UK. [†]Present addresses: Center for Infectious Diseases, Parasitology, Heidelberg University Hospital, INF 345, 69120 Heidelberg, Germany (M.G.); Division of Infectious Diseases, Boston Children's Hospital and Department of Pediatrics, Harvard Medical School, Boston, Massachusetts 02115, USA (J.D.D.); Department of Biochemistry, Molecular Biology, Entomology and Plant Pathology, Mississippi State University, Starkville, Mississippi 39762, USA (J.G.K.); Department of Global Health and Center for Drug Discovery and Innovation, University of South Florida, Tampa, Florida 33612 USA (R.H.Y.J.); Department of Infectious Diseases and Pathology, College of Veterinary Medicine, University of Florida, Gainesville, Florida 32611, USA (R.R.D.). *e-mail: mduraisi@hsph.harvard.edu

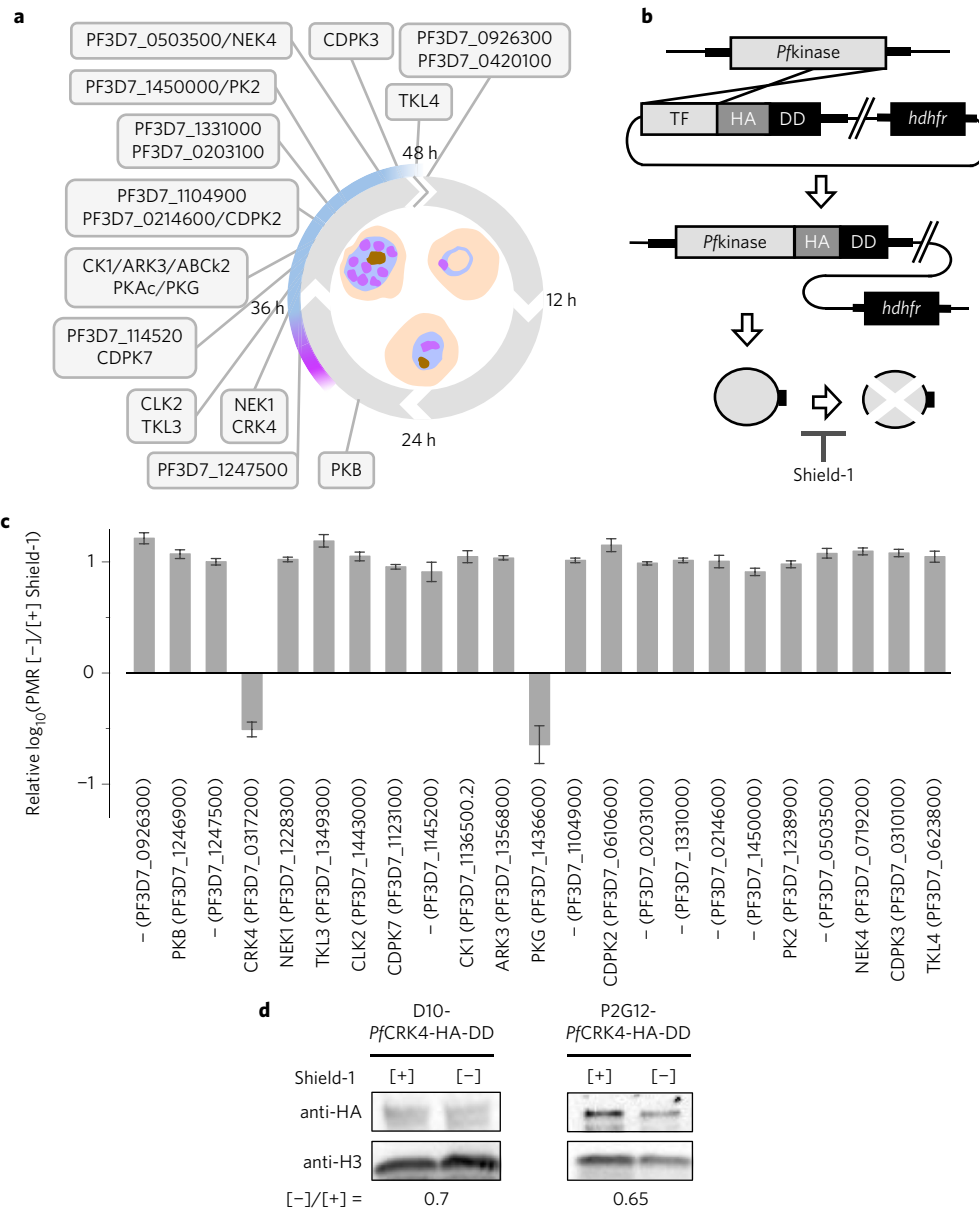


Figure 1 | Conditional destabilization identified *P. falciparum* CRK4 as essential for asexual blood-stage development. **a**, Schematic of the *P. falciparum* blood-stage cycle indicating peak transcript times of kinases targeted with a destabilization domain. Purple, approximate onset of DNA replication; blue, approximate duration of schizogony. **b**, Single-crossover 3' replacement strategy to fuse candidate kinases with a haemagglutinin (HA) and a destabilization domain (DD) tag, which destabilizes kinases in the absence of Shield-1. Note that PKAc, ABCK2 and PF3D7_0420100 were refractory to HA-DD fusion. TF, targeting fragment. **c**, Effect of conditional kinase destabilization on parasite growth over two cycles (\pm s.d.). PMR, parasite multiplication rate. **d**, Western blots demonstrate conditional destabilization of *PfCRK4* in two genetic backgrounds. The level of knockdown is indicated below. H3, histone H3.

segmented into daughter cells containing nuclei and rhoptries (apical organelles required for merozoite invasion), which are characteristic of mature schizonts (Fig. 2d, top). In contrast, parasites cultured [-] Shield-1 (that is, *PfCRK4* is depleted) showed no nuclear division or apical organelle biogenesis (Fig. 2d bottom and Supplementary Fig. 5a).

Analysis of nuclei stained with fluorescent DNA-specific dyes confirmed that the nuclei did not divide and revealed a substantially distorted nuclear morphology (Fig. 2e and Supplementary Fig. 5b). Hemispindle structures were evident in *PfCRK4*-depleted cells (Fig. 2f and Supplementary Fig. 5c,d); however, they were greatly enlarged relative to spindles in wild-type parasites and might account for the nuclear distortion. Concordantly, division of the centriolar plaque^{3,21}, the parasite's microtubule organizing centre, was diminished (Fig. 2g). To ascertain whether *PfCRK4* affects

DNA replication, we quantified the parasite's DNA content by flow cytometry^{22,23}. In wild-type parasites, DNA replication commences at 29–32 h.p.i. (that is, parasites with *C*-values >1 appear), but we found DNA replication to be profoundly inhibited in *PfCRK4*-depleted parasites (Fig. 2h). In contrast, the development of the mitochondria and apicoplast organelles was unaffected following depletion of *PfCRK4* (Supplementary Fig. 5e,f). The *PfCRK4*-dependent block was completely reversible up to 38 h.p.i. by the addition of Shield-1. However, reversion at 48 h.p.i. led to very poor recovery (Fig. 2i), identifying a window within which *PfCRK4* depletion is cytostatic before becoming cytotoxic.

To elucidate the processes regulated by *PfCRK4*, we assessed changes in the phosphoproteome of *PfCRK4*-depleted parasites at two time points (Fig. 3a): at 29 h.p.i., when *PfCRK4* is already expressed at the onset of DNA replication (Fig. 2b,h) and also at 37 h.p.i., where in

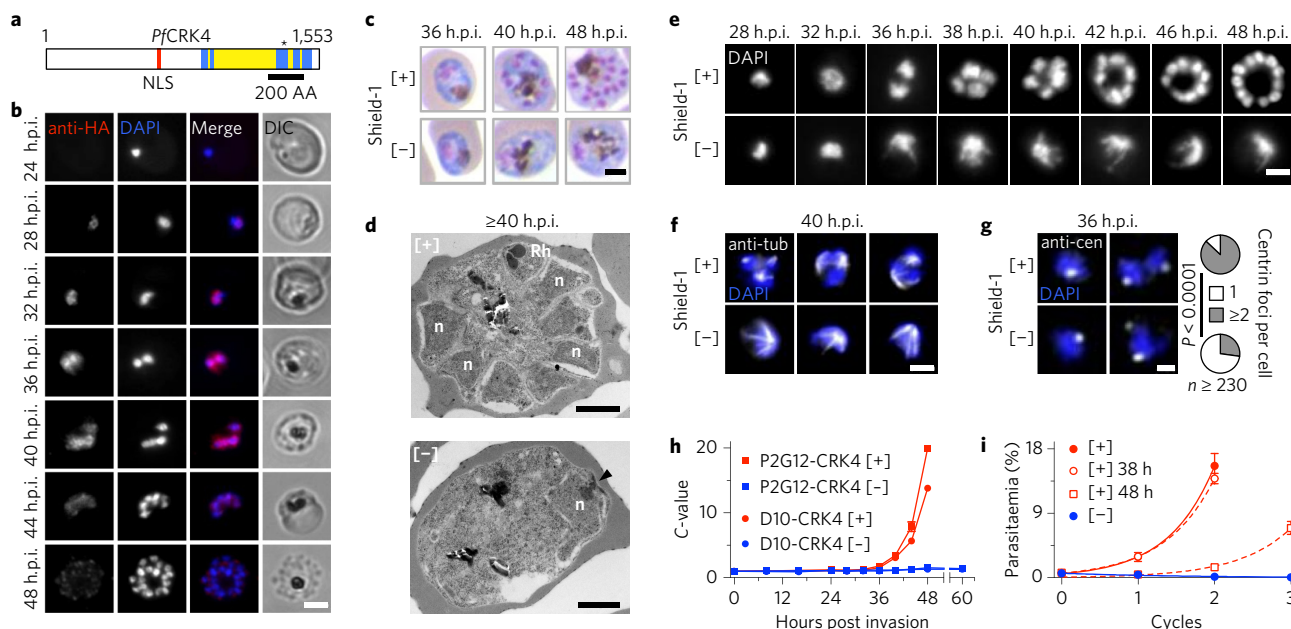


Figure 2 | Nuclear-localized *PfCRK4* is essential for the trophozoite-to-schizont transition and DNA replication. **a**, Domain structure of *PfCRK4*. Blue, kinase domain; yellow, kinase domain insertions relative to human CDK2; red, predicted nuclear localization signal (NLS); asterisk, active site residues; 1 and 1,553, first and last amino acid (AA), respectively. **b**, Immunofluorescence detection of *PfCRK4*-HA-DD in blood-stage parasites (representative of three biological replicates). DIC, differential interference contrast. Scale bar, 3 μ m. **c**, Light microscopy of May-Grünwald-Giemsa-stained *PfCRK4*-depleted parasites (D10 parent, representative of two biological replicates and results with P2G12-*PfCRK4*-HA-DD). Scale bar, 2 μ m. **d**, Ultrastructure of *PfCRK4*-depleted parasites (D10 parent, representative of $n \geq 25$ cells per condition). Arrowhead, spindle pole body; n, nucleus; Rh, rhoptry. Scale bars, 1 μ m. **e**, Nuclear development in *PfCRK4*-depleted parasites (D10 parent, representative of three biological replicates, and results with P2G12-*PfCRK4*-HA-DD). Scale bar, 2 μ m. **f**, Immunofluorescence detection of spindle structures in *PfCRK4*-depleted parasites (P2G12 parent, representative of two biological replicates). Tub, tubulin. Scale bar, 2 μ m. **g**, Quantification of centriolar plaques by immunofluorescence in *PfCRK4*-depleted parasites (D10 parent; P value, chi-square test; representative of two biological replicates and results with P2G12-*PfCRK4*-HA-DD). Cen, centrin. Scale bar, 1 μ m. **h**, DNA content of *PfCRK4*-depleted parasites from both parental lines; mean \pm s.d. of technical triplicates (representative of three biological replicates); ring-stage DNA content defined as 1 (C-value). **i**, Proliferation of parasites when *PfCRK4* was re-stabilized from 38 h.p.i. or 48 h.p.i. of the first cycle onwards; mean \pm s.d. (representative of two biological replicates and results with P2G12-*PfCRK4*-HA-DD).

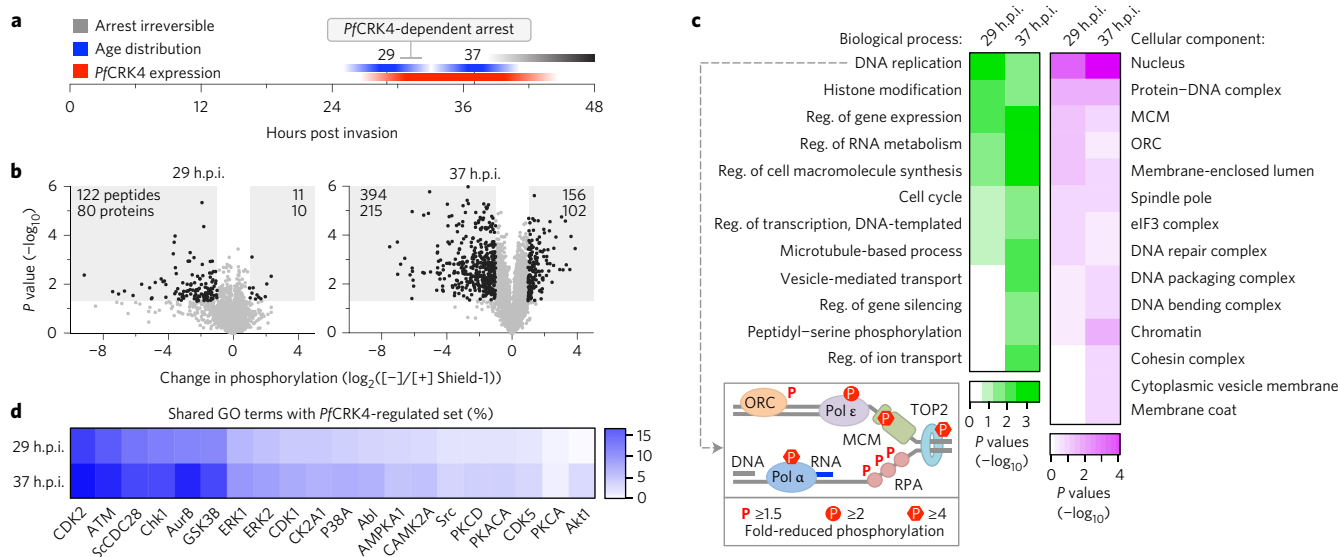


Figure 3 | *PfCRK4* regulates S phase. **a**, Schematic illustrating the sampling time points for phosphoproteomic profiling. **b**, Differential phosphorylation in D10-*PfCRK4*-HA-DD parasites [-] Shield-1 relative to [+] Shield-1; 29 h.p.i. in duplicate, 37 h.p.i. in triplicate. P values, Student's t -test. Grey-shaded regions indicate >2 -fold changes in phosphorylation and $P < 0.05$. Numbers of peptides and respective proteins are indicated. **c**, GO term enrichment analysis of proteins with ≥ 2 -fold-reduced phosphorylation ($P < 0.05$). P values, modified Fisher's exact test. Box shows *P. falciparum* homologues of *S. cerevisiae* factors required for origin of replication activation *in vitro* with reduced phosphorylation at 37 h.p.i. in *PfCRK4*-depleted parasites. Pol, DNA polymerase; MCM, mini-chromosome maintenance complex; TOP2, topoisomerase 2; RPA, replication protein A; ORC, origin recognition complex; eIF3, eukaryotic initiation factor 3. **d**, Percentage of shared GO terms of proteins with ≥ 2 -fold-reduced phosphorylation ($P < 0.05$) upon *PfCRK4*-depletion and of substrate sets of human and *S. cerevisiae* (Sc) kinases.

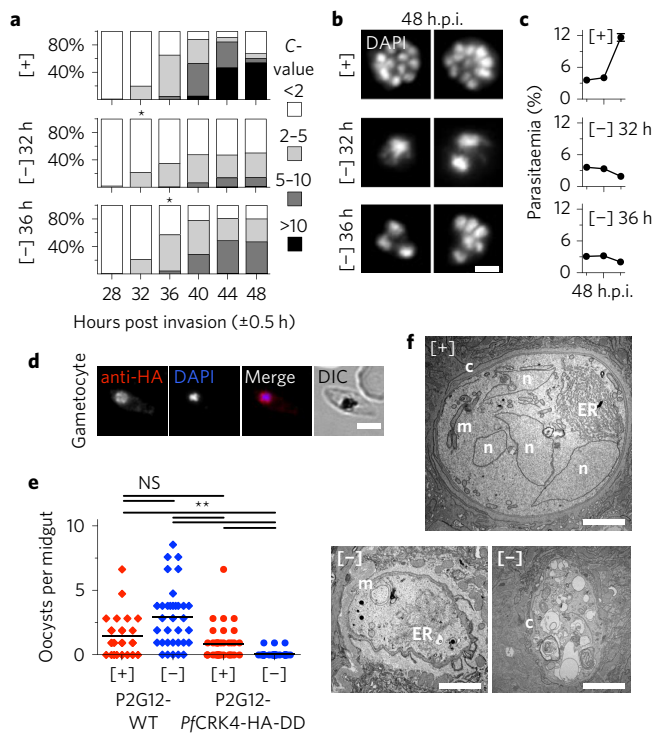


Figure 4 | *PfCRK4* is essential throughout schizogony and critical for transmission. **a**, DNA content analysis of D10-*PfCRK4*-HA-DD parasites when *PfCRK4* was present or depleted from 32 h.p.i. or 36 h.p.i. onwards. 1 (C-value), ring-stage DNA content; asterisks, time of Shield-1 removal (representative of two biological replicates and results with P2G12-*PfCRK4*-HA-DD). Note: second-cycle ring-stage parasites reappear at 48 h.p.i. when *PfCRK4* is present. **b**, DAPI-stained nuclei of parasites from **a** (representative of $n \geq 70$ cells per condition). Scale bar, 2 μm . **c**, Proliferation of cultures from **a** (mean \pm s.d. of triplicates). **d**, Immunofluorescence detects *PfCRK4*-HA-DD in gametocytes (P2G12 parent, representative of two biological replicates). Scale bar, 4 μm . **e**, Depletion of *PfCRK4* during gametocytogenesis diminished oocyst numbers on *An. gambiae* female midguts. Bars, mean oocyst numbers; NS, not significant; ** $P \leq 0.01$ (Kruskal-Wallis test). **f**, Ultrastructure of mosquito-stage parasites from infections with *PfCRK4*-depleted gametocytes (P2G12 parent, representative of ≥ 10 cells from independent infection experiments). ER, endoplasmic reticulum; n, nucleus; m, mitochondria; c, capsule. Scale bars, 1 μm .

wild-type parasites DNA replication is evident and when the *PfCRK4*-dependent arrest is still reversible (Fig. 2h,i, Supplementary Fig. 6 and Supplementary Data 2–5). Large changes occur in the phosphoproteome at 29 h.p.i., indicating that *PfCRK4* is active when the first round of DNA replication commences (Fig. 2h). We used k-means clustering to identify the phosphorylation sites most affected by the *PfCRK4* depletion, which showed a reduction of about 2-fold (Supplementary Fig. 6b). Applying a threshold based on a ≥ 2 -fold decrease in phosphorylation and P values of < 0.05 , we identified 220 proteins (80 from 29 h.p.i. and 215 from 37 h.p.i., with 75 proteins shared), suggesting that these belong to a *PfCRK4*-regulated set of phosphoproteins (Fig. 3b and Supplementary Data 4). Western blot analysis confirmed differential phosphorylation of histone H3 (serine 28) in a different genetic background (Supplementary Fig. 6c). The most enriched phosphorylation motif within these proteins was a previously undescribed S Φ xK motif (Φ , hydrophobic; x, any amino acid), with S being phosphorylated. The canonical CDK motif S/TP (refs 24,25), with S or T phosphorylated, was also enriched (Supplementary Fig. 6d,e).

To examine the functional significance of the *PfCRK4*-regulated set of proteins, we used gene ontology (GO) term enrichment analysis

(Fig. 3c). The most enriched biological-process GO term was ‘DNA replication’, and ‘nucleus’ was the most enriched cellular-component GO term. Strikingly, six of the seven identifiable *P. falciparum* homologues (or subunits thereof) of the 16 *Saccharomyces cerevisiae* factors required for origin licensing and firing *in vitro*²⁶ showed reduced phosphorylation in *PfCRK4*-depleted parasites (Fig. 3c box, Supplementary Fig. 6f and Supplementary Data 3 and 4). GO terms of proteins with a ≥ 2 -fold increase in phosphorylation ($P < 0.05$) were enriched for biosynthetic and intracellular transport processes at 37 h.p.i., perhaps indicating secondary effects, but no statistically significant enrichment was observed at 29 h.p.i. (Supplementary Fig. 6g).

We next compared the GO terms of the *PfCRK4*-regulated set with GO terms of other available kinase substrate sets—one *S. cerevisiae* kinase²⁷ and 19 human kinases²⁸ (www.phosphosite.org)—each with ≥ 30 confirmed substrates (Fig. 3d). The substrate set of human CDK2, a major S-phase promoting factor, showed the highest percentage of shared annotations, suggesting that *PfCRK4* acts in a related fashion to promote the S phase in *P. falciparum*.

PfCRK4 protein levels increased through early and mid schizogony (Fig. 2b) and its transcripts peak the latest of all putative *Plasmodium* CDK-like kinases²⁹. We therefore hypothesized that *PfCRK4* is crucial for all rounds of DNA replication seen in schizogony. When we depleted *PfCRK4* at points later in schizogony, we detected no further increase in DNA content (Fig. 4a), premature termination of nuclear division (Fig. 4b), and the parasites failed to proliferate (Fig. 4c), thus demonstrating that *PfCRK4* function is critical throughout schizogony.

To determine a role for *PfCRK4* in other life-cycle stages, we used the P2G12-*PfCRK4*-HA-DD line that produces high levels of gametocytes to analyse *PfCRK4* function during parasite transmission to the *Anopheles gambiae* mosquito vector. Although we detected nuclear expression of *PfCRK4* in gametocytes (Fig. 4d and Supplementary Fig. 7a), depletion during the latter portion of gametocyte development (that is, from day 6 to day 16 post-induction) had no effect on gametocytaemia nor on the male-to-female gametocyte ratio (Supplementary Table 1). *PfCRK4* depletion also did not impair exflagellation (Supplementary Fig. 7b–d). We observed a reduced *PfCRK4* signal in ookinetes (Supplementary Fig. 7e), and the numbers of oocysts on *An. gambiae* female midguts was greatly diminished following *PfCRK4* depletion (Fig. 4e and Supplementary Fig. 8). Oocysts derived from gametocyte cultures in the presence of *PfCRK4* showed multiple nuclei, well-expanded organelles and a well-developed capsule (Fig. 4f, top). In contrast, infections with *PfCRK4*-depleted gametocytes resulted in necrotic parasites reminiscent of dead ookinetes, the motile zygote of *Plasmodium* parasites (Fig. 4f bottom and Supplementary Fig. 8). This indicates that *PfCRK4* is required at some point during ookinete formation and early oocyst development, and might play a role during DNA replication in zygotes.

Our data provide evidence that *PfCRK4* is an essential protein kinase promoting S phase through the initiation of multiple rounds of DNA replication during schizogony. Phosphorylation is probably important for the regulation of *PfCRK4* (Supplementary Figs 3b and 4a), but a potential cyclin dependence is in question, as the cyclin-binding domain is poorly conserved (Supplementary Fig. 4a)¹⁷. Interestingly, homologues of Group I cyclins are not found in the *Plasmodium* genome, including cyclin E, which is critical for the G1/S transition in other organisms³⁰. Interventions targeting *PfCRK4* function would be efficacious throughout the extended period of schizogony in the clinically relevant blood stage, as well as in the transmission stages, which taken together are attractive features for future drug development.

Methods

Reagents and oligonucleotide primers. We purchased chemicals from Sigma-Aldrich (unless otherwise noted), primers from Integrated DNA Technologies (sequences are available upon request) and restriction enzymes from New England Biolabs.

Construction of plasmids. The terminal 1–2 kb of PKB (PF3D7_1246900), TLK4 (PF3D7_0623800) and PKG (PF3D7_1436600) were subcloned into the 3' replacement vector pJDD41 (ref. 7), generating HA-DD single-crossover tagging plasmids. The terminal ~1 kb of PF3D7_0420100 was amplified using an extended reverse primer, introducing two additional HA-tags. Cloning into pJDD41 resulted in a 3xHA-DD single-crossover tagging plasmid. All other targeting fragments were subcloned into this 3xHA-DD plasmid (sequences available upon request).

Parasite culture, transfection and synchronization. *P. falciparum* D10 was obtained from the Walter and Eliza Hall Institute (Melbourne, Australia). *P. falciparum* P2G12 (clone of 3D7) was obtained from Harvard T.H. Chan School of Public Health (Boston, USA). Parasites were cultured as previously described in RPMI 1640 medium supplemented with 0.5% Albumax-II (Invitrogen), 50 mg l⁻¹ hypoxanthine, 0.21% sodium bicarbonate and 25 mM HEPES (EMD Biosciences)³¹. Human O+ erythrocytes (Research Blood Components) were diluted to 2–4% haematocrit. Transgenic parasites were generated by electroporation of synchronized ring-stage parasites as previously described³². Single homologous recombination events were selected in the presence of 500 nM Shield-1 by cycling WR99210 (Jacobus Pharmaceutical Company) on and off, and cloned by limiting dilution. Parasites were synchronized by a combination of heparin and sorbitol treatments as previously described³³. Unless otherwise noted, DD-tagged parasites were cultured in 250 nM Shield-1. When desired, Shield-1 was removed by triple washes with excess RPMI.

Southern blot analysis. Genomic DNA was collected with a QIAamp Blood Mini Kit (Qiagen) and digested with the enzymes indicated in Supplementary Fig. 1a, resolved on 0.8% agarose gels, transferred to GeneScreen Plus (Perkin Elmer) and hybridized with specific radiolabelled probes.

May-Grünwald-Giemsa staining and imaging of blood-stage parasites. Air-dried thin-smear blood films were fixed and stained according to manufacturers' instructions and imaged on a Zeiss AxioCam microscope equipped with a ×100 oil-immersion objective. Raw images were analysed using ImageJ (ref. 34).

Dose response experiments. Dose response curves were generated as previously described using SYBR Green I (ref. 35). In brief, triplicate twofold Shield-1 dilution series were set up in 100 µl parasite cultures (0.075% parasitaemia in 2% haematocrit). After two cycles, parasites were lysed with 20 µl of 6× SYBR green I lysis buffer (0.16% saponin; 20 mM Tris-HCl, 5 mM EDTA, 1.6% Triton X-100, pH 7.4), supplemented with 1:1,000 SYBR green I (from 10,000× stock, Thermo Fisher). Fluorescence intensity was measured on a SpectraMax M5 plate reader (Molecular Devices).

Conditional destabilization screen of schizont-stage kinases. We used the relative log₁₀ parasite multiplication rate (PMR) [-] over [+] Shield-1 as a measure of the effect of conditional destabilization of schizont-stage kinases. Synchronized ring-stage parasites of all *P. falciparum* kinase-DD fusion lines were seeded in triplicate at 0.05% parasitaemia, 0.5% haematocrit [+] or [-] Shield-1. Parasitaemia was monitored by flow cytometry (see below) and expressed as log₁₀. Linear regression analysis (Prism, GraphPad) allowed PMR to be calculated. The effect of protein knockdown ([-] Shield-1) relative to [+] Shield-1 was plotted as log₁₀ PMR [-] Shield-1 over log₁₀ PMR [+] Shield-1. The error (standard deviation, s.d.) for

$$f = \frac{A}{B}$$

where *A* is log₁₀ PMR [-] Shield-1 and *B* is log₁₀ PMR [+] Shield-1, was propagated as

$$s_f = |f| \sqrt{\left(\frac{s_A}{A}\right)^2 + \left(\frac{s_B}{B}\right)^2}$$

where *s_A* and *s_B* are the sample standard deviations in *A* and *B*, respectively³⁶.

Parasitaemia quantification by flow cytometry. Parasitized erythrocytes were fixed as described previously³⁷, stained with 1:2,000 SYBR green I (Life Technologies) in PBS and analysed on a Miltenyi MACSQuant flow cytometer. Data were analysed using FlowJo (Tree Star) and Prism (GraphPad) software.

Immunoblot analysis. Synchronized parasites were collected and uninfected erythrocytes were removed using 0.05% saponin in PBS plus 1× cOmplete protease inhibitor cocktail (Roche). Following washes, parasites were lysed in Laemmli sample buffer and proteins were resolved by SDS-PAGE, transferred to nitrocellulose and probed with the following primary antibodies: anti-HA (1:1,000, Roche, clone 3F10), anti-Pf lactate dehydrogenase (LDH) (1:2,000, gift from M.T. Makler), anti-histone H3 (1:1,000, Abcam, ab1791), anti-pS28 histone H3 (1:1,000, Abcam, ab5169) anti-Pf aldolase (1:40,000, Abcam, ab38905). Signal intensities were quantitated using ImageJ.

Gametocyte assays and *An. gambiae* infections. Gametocyte cultures were seeded at 0.5% parasitaemia in 5 ml RPMI with 10% serum, 4% haematocrit and 1 µM Shield-1 and kept in a candle jar at 37 °C. From day six onwards, parasites were cultured [+] and [-] Shield-1. Estimates for the various stages and sexes were determined from a Giemsa-stained thin-smear blood film. On days 15 to 18 of culture, parasites were collected and male gametocyte exflagellation was assessed by microscopy. For the infection of *An. gambiae* KEELE strain females, cultures were washed and gametocytaemia was adjusted to 0.3% in normal human serum with 45% haematocrit. Subsequently, females were infected in a standard membrane feeding assay as previously described³⁸.

Oocyst quantification. Midguts from infected *An. gambiae* females were dissected on days 7 or 8 post blood-feeding, and the number of oocysts were then enumerated following 0.1% mercurochrome staining and analysis by light microscopy (×20 objective).

DNA content analysis. The DNA content of parasites was determined by flow cytometry. Parasitized erythrocytes were fixed in 4% paraformaldehyde and 0.0075% glutaraldehyde for 45 min at room temperature³⁷. To reduce the RNA-derived background signal, cells were permeabilized with 0.1% Triton X-100, treated with 0.3 mg ml⁻¹ RNase A for 20' at 37 °C and subsequently washed. Cells were stained with 1:2,000 SYBR green I (Life Technologies) in PBS, washed, and analysed on a Miltenyi MACSQuant flow cytometer. Data were analysed using FlowJo (Tree Star), Excel (Microsoft) and Prism (GraphPad) software. Second-cycle ring-stage parasites were omitted for DNA content analysis of 48 h.p.i. schizont-stage parasites.

Immunofluorescence assays. Immunofluorescence assays of blood-stage parasites was carried out as previously described^{37,39}. In brief, parasitized erythrocytes were air-dried, methanol-fixed³⁹, and analysed using rat anti-HA (1:100, Roche, clone 3F10), mouse anti-centrin (1:500, Millipore, clone 20H5), mouse anti-α-tubulin (1:2,000, Sigma-Aldrich, clone B-5-1-2), rabbit anti-PfGAP45 (1:2,000, gift from J.C. Rayner) or rabbit anti-PfEBA175 (1:500, Malaria Research and Reference Reagent Resource Center, R3347) antibodies. Alternatively, parasites were fixed in solution³⁷ for 20 min at room temperature, immobilized on poly-L-lysine coated coverslips (Corning), and analysed using mouse anti-α-tubulin (1:2,000, Sigma-Aldrich, clone B-5-1-2) or rabbit anti-PfACP⁴⁰ (1:500, gift from S.T. Prigge) antibodies. Primary antibodies were detected using Alexa Fluor-conjugated secondary antibodies (1:2,000, Thermo Fisher Scientific). Cells were mounted with DAPI (4',6-diamidino-2-phenylindole) Fluoromount-G (SouthernBiotech) or cells were stained with Hoechst 33342 (Thermo Fisher Scientific) and mounted with Fluoromount-G (SouthernBiotech), imaged on a Nikon Eclipse TE300 microscope equipped with a Hamamatsu C10600 Orca R2 digital camera, and analysed using ImageJ software.

For immunofluorescence analysis of exflagellation, mature gametocytes were resuspended in RPMI 1640 medium supplemented with 20% human serum (AB+), 50 mg l⁻¹ hypoxanthine, 0.21% sodium bicarbonate, 25 mM HEPES (EMD Biosciences) and 50 µM xanthurenic acid at room temperature and pH 8 to induce exflagellation⁴¹. Following 20 min incubation at room temperature, cells were washed, spotted on a glass slide, air-dried, methanol-fixed and processed further as described above.

For immunofluorescence analysis of ookinetes, female *An. gambiae* mosquitoes were fed with late-stage PfCRK4-HA-DD gametocyte cultures, which were maintained [+] and [-] Shield-1 from day 6 post-induction. Approximately 24 h post-feeding, the blood bolus from the mosquito midgut lumen was isolated. Bolus material was spotted on glass slides and air-dried before immunofluorescence analysis.

Immunofluorescence analysis of *P. falciparum* late midgut oocysts was done as previously described⁴². In brief, dissected midguts were fixed in 4% paraformaldehyde for 1 h at room temperature, washed, permeabilized and blocked using 0.2% Triton X-100 in 1% bovine serum albumin in PBS. Midgut oocysts were analysed using a mouse anti-circumsporozoite (CS) protein antibody (15 µg ml⁻¹, gift of P. Sinnis), an Alexa Fluor 594 secondary antibody (1:1,000) and DAPI nuclear stain, mounted on a glass slide in 10% glycerol in PBS and imaged on a Nikon Eclipse 90i microscope. Raw images were analysed using Velocity software (Perkin-Elmer).

JC-1 staining of *P. falciparum* mitochondria. Parasite mitochondria were stained with the cationic mitochondrial membrane potential sensor JC-1 (Life Technologies) as previously described⁴³. In brief, 2 µM JC-1 in 37 °C warm RPMI was filtered using an Acrodisc Syringe Filter (0.2 µm HT Tuffryn Membrane, Pall) to removed preformed JC-1 aggregates. Parasites were incubated with JC-1-containing medium for 20 min at 37 °C, washed, and imaged immediately on a Nikon Eclipse TE300 microscope equipped with a Hamamatsu C10600 Orca R2 digital camera and analysed using ImageJ software.

Electron microscopy. Synchronized blood-stage parasites were isolated by magnetic affinity purification using a MACS LS column (Miltenyi Biotec), adjusted to ~50% parasitaemia with uninfected erythrocytes and resuspended in 200 µl 3% BSA in PBS. Cells were fixed for 1 h at room temperature with an equal volume of 2.5% paraformaldehyde, 5.0% glutaraldehyde and 0.06% picric acid in 0.2 M cacodylate

buffer. Cells were washed in cacodylate buffer, post-fixed for 1 h with 1% osmium tetroxide (OsO_4), 1.5% potassium ferrocyanide ($\text{K}_3\text{Fe}(\text{CN})_6$) and washed in H_2O . Following 1 h incubation in 1% aqueous uranyl acetate solution, samples were washed in H_2O and subsequently dehydrated in grades of alcohol. The samples were placed in propyleneoxide for 1 h and infiltrated in a 1:1 mixture of propyleneoxide and TAAB Epon (Marivac) over night. Samples were embedded in TAAB Epon and polymerized at 60 °C for 48 h. Ultrathin sections from a Reichert Ultratuc-S microtome were mounted on copper grids and stained with lead citrate. Samples were imaged on a Tecnai G2 Spirit BioTWIN with an AMT 2k charge-coupled device camera under 80 kV.

For *P. falciparum* oocyst thin-section transmission electron microscopy, infected midguts were fixed at day 7 post-infection in 2.5% glutaraldehyde (Electron Microscopy Sciences) and processed as described in ref. 44. Stained sections were examined with a Philips CM120 electron microscope under 80 kV.

Phosphoproteomic profiling

Cell culture and collection. Synchronized D10-*PfCRK4*-HA-DD parasites were cultured for 29 or 37 h.p.i. [+] or [-] Shield-1. At 29 h.p.i., duplicate samples were collected, and at 37 h.p.i., triplicate samples were collected for both [+] and [-] Shield-1. For each of the ten samples, $\sim 1.25 \times 10^9$ parasites were isolated, and uninfected erythrocytes were removed using saponin buffer (0.05% saponin in PBS plus 1× PhosSTOP (Roche), 1× cOmplete protease inhibitor cocktail (Roche) and 1 mM phenylmethanesulfonyl fluoride (PMSF)). Subsequently, cells were washed in saponin buffer to further remove erythrocytes and erythrocyte debris, followed by washes with PBS plus 1× PhosSTOP, 1× cOmplete protease inhibitor cocktail and 1 mM PMSF.

Cell lysis and protein digestion. Lysates were prepared as previously described^{45,46}. In brief, cells were lysed in 8 M urea, 100 mM sodium chloride, 25 mM TRIS pH 8 plus 1× PhosSTOP, 1× cOmplete protease inhibitor cocktail and 1 mM PMSF in PBS. The protein concentration was estimated in the Bio-Rad Protein Assay (Bio-Rad). Disulfide bonds were reduced with 5 mM tris(2-chloroethyl) phosphate (TCEP) for 30 min at 37 °C. Cysteines were alkylated with 15 mM iodoacetamide for 30 min at room temperature in the dark, followed by incubation with 5 mM dithiothreitol (DTT) for 15 min at room temperature in the dark to quench excess iodoacetamide.

Chloroform-methanol precipitated proteins⁴⁷ were resuspended in 8 M urea, 50 mM HEPES pH 8.5 and subsequently diluted to 1 M urea 50 mM HEPES pH 8.5 for digestion with LysC protease (1:100 protease-to-protein ratio, 3 h at 37 °C) before the addition of trypsin (1:100 protease-to-protein ratio) and continued digest overnight at 37 °C. The reaction was quenched with 1% formic acid, subjected to C18 solid-phase extraction (Sep-Pak, Waters), followed by vacuum-centrifugation.

Isobaric labelling with tandem mass tags (TMTs). Peptides (200 µg) from each sample were dissolved in 100 mM HEPES pH 8.5. Labelling with TMT reagents (Thermo Fisher Scientific) was carried out according to the manufacturer's instructions and as previously described⁴⁸. The TMT-labelled samples were combined in a 1:1 ratio across all samples, vacuum centrifuged to near dryness, and subjected to C18 solid-phase extraction (Sep-Pak, Waters).

Phosphopeptide enrichment. Peptides were resuspended in 100 mM HEPES pH 8.5 and phosphopeptides were enriched using Titanosphere TiO_2 5 µm particles (GL Biosciences) as previously described^{46,48,49}. The flow-through was kept for proteome analysis. Enriched TMT-labelled phosphopeptides and peptides were dried by vacuum centrifugation.

Offline basic pH reversed-phase (BPRP) fractionation. For protein level analysis, we fractionated the pooled TMT-labelled peptide sample via BPRP high-performance liquid chromatography as previously described^{48,50}. Fractions were desalted, dried and reconstituted in 5% acetonitrile, 5% formic acid for mass spectrometry processing.

For phosphopeptide analysis, we used the Pierce Off-line BPRP fractionation kit (Thermo Scientific). Fractions collected included organic buffer bumps with 5, 7.5, 10, 12.5, 15, 17.5, 20, 50 and 70% acetonitrile, in addition to the wash and flow through fractions. These fractions were vacuum-centrifuged to near dryness, desalted via StageTip, dried and reconstituted in 5% acetonitrile/5% formic acid for LC-MS/MS processing.

Liquid chromatography and tandem mass spectrometry. Data were collected using an Orbitrap Fusion mass spectrometer (Thermo Fisher Scientific) coupled to a Proxeon EASY-nLC II liquid chromatography (LC) pump (Thermo Fisher Scientific). Peptides were fractionated on a 75 µm inner diameter microcapillary column packed with ~ 0.5 cm Magic C4 resin (5 µm, 100 Å, Michrom Bioresources) followed by ~ 35 cm GP-18 resin (1.8 µm, 200 Å, Sepax). For each analysis, we loaded ~ 1 µg onto the column.

For total proteome analysis, peptides were separated using a 180 min gradient of 6–23% acetonitrile in 0.125% formic acid (flow rate of ~ 600 nl min⁻¹). Each analysis used the multi-notch MS3-based TMT method⁵¹. The scan sequence began with an MS1 spectrum (Orbitrap analysis; resolution of 120,000, mass range of 400–1,400 *m/z*, automatic gain control (AGC) target of 2.0×10^5 , maximum injection time of 100 ms). Precursors for MS2/MS3 analysis were selected using a

TopSpeed 2 s method. MS2 analysis consisted of collision-induced dissociation (quadrupole ion trap analysis: AGC of 4×10^3 , normalized collision energy (NCE) of 35, maximum injection time of 150 ms). Following acquisition of each MS2 spectrum, we collected an MS3 spectrum using a recently described method in which multiple MS2 fragment ions were captured in the MS3 precursor population using isolation waveforms with multiple frequency notches⁵¹. MS3 precursors were fragmented by high-energy collision-induced dissociation (HCD) and analysed (NCE 55: AGC of 5×10^4 , maximum injection time of 150 ms, resolution of 60,000 at 200 Th).

For phosphoproteome analysis, peptides were separated using a 120 min gradient of 3–23% acetonitrile in 0.125% formic acid (flow rate of ~ 575 nl min⁻¹). Each analysis used the multi-notch MS3-based TMT method⁵¹. The scan sequence was identical to the proteome scan, except the maximum injection time was 200 ms for MS2 analysis and 250 ms for MS3 analysis.

Initial mass spectrometry data analysis. Mass spectra were processed using a SEQUEST-based in-house software pipeline⁵². Spectra were converted to mzXML using a modified version of ReAdW.exe. Database searching included all entries from a combined Uniprot human and *Plasmodium* database (February 2015). This database was concatenated with one composed of all protein sequences in the reversed order. Total protein level analysis searches were performed using a 50 ppm precursor ion tolerance, and product ion tolerance was set to 0.9 Da. These wide mass tolerance windows were chosen to maximize sensitivity in conjunction with SEQUEST searches and linear discriminant analysis^{52,53}. TMT tags on lysine residues and peptide N termini (+229.163 Da) and carbamidomethylation of cysteine residues (+57.021 Da) were set as static modifications, while oxidation of methionine residues (+15.995 Da) was set as a variable modification for both total proteome and phosphoproteome data sets. For phosphoprotein analysis, +79.966 Da was set as a variable modification on serine, threonine and tyrosine residues.

Peptide-spectral matches (PSMs) were adjusted to a 1% false discovery rate (FDR)^{54,55}. PSM filtering used a linear discriminant analysis as previously described⁵², while considering the following parameters: XCorr, ΔCn, missed cleavages, peptide length, charge state and precursor mass accuracy. For the phosphorylation data set, site localization was evaluated via AScore⁵³. For TMT-based reporter ion quantitation, we extracted the summed signal-to-noise (S/N) ratio for each TMT channel and found the closest matching centroid to the expected mass of the TMT reporter ion.

The search space for each reporter ion was limited to a range of 0.003 Th to prevent overlap between the isobaric reporter ions. For protein-level comparisons, PSMs were identified, quantified, collapsed to a 1% peptide FDR, and further collapsed to a final protein-level FDR of 1%. Protein assembly was guided by principles of parsimony to produce the smallest set of proteins necessary to account for observed peptides.

Proteins were quantified by summing reporter ion counts across all matching PSMs using in-house software, as previously described⁵². Poor-quality PSMs, MS3 spectra with >8 TMT reporter ion channels missing, MS3 spectra with TMT reporter summed S/N ratio <100, or no MS3 spectra were excluded from quantitation⁵¹. Protein quantitation values were exported for further analysis in Microsoft Excel or SAS JMP. Each reporter ion channel was summed across all quantified proteins and normalized assuming equal protein loading of all ten samples.

Evolutionary relationship of *PfCRK4*. Protein kinase amino acid sequences from the cyclin-dependent kinase (CDK) families of apicomplexans and model organism and non-CDK out-group kinases were chosen for comparison with *PfCRK4* (Supplementary Data 1). Kinase domain sequences were trimmed, aligned using MUSCLE⁵⁶ and analysed using RAXML⁵⁷.

Domain drawings of *PfCRK4* and its orthologues in *Plasmodium* spp. Domain boundaries were identified by searching sequences against Pfam⁵⁸ using the HMMER package⁵⁹. Domains were illustrated using ProtDraw (<http://sourceforge.net/projects/protdraw/>).

Homology modelling of *PfCRK4*. The protein kinase domain of *PfCRK4* was modelled using the co-crystal structure of the human CDK2-cyclin A-substrate peptide complex (1QMZ.pdb)²⁵. We used this structure as a template to model *PfCRK4* in a potentially active form. The kinase domains of the target and query sequences were aligned using MUSCLE⁵⁶ followed by manual review and adjustment. Homology models were made using MODELLER 9.15 (ref. 60). Structural alignments were reviewed and adjusted using Chimera⁶¹.

Identification of conditionally related clusters in proteomic and phosphoproteomic data. The total sum S/N values of peptides collapsed into proteins are given in Supplementary Data 3. For phosphopeptides values see Supplementary Data 4. Contaminants and false positives were removed and values for each channel were normalized by the column sum. Values were placed on a scale of 0–1 by dividing by the maximum value for the protein or phosphopeptide. Scaling was done for all channels at once and separately for experiments at 29 h.p.i. and 37 h.p.i. Phosphopeptides for a total sum S/N ≤ 100 were not included in clustering analysis and the total sum S/N values were adjusted to reflect protein levels from the

proteome analysis. K-means clustering⁶² was done using R (<http://cran.r-project.org/>) with the Hartigan–Wong method using 1,000 starting configurations and 10,000 iterations. Clustering results, log₂-fold changes, and -log₁₀ *P* values (Student's *t*-test) are included in Supplementary Data 3 and 4.

Gene orthology relationships. Relationships between *P. falciparum* proteins and *S. cerevisiae* orthologues for the box in Fig. 3f (Supplementary Data 3) were investigated using a downloaded version of the OrthoMCL database, version 5 (ref. 63). A comprehensive orthology analysis is provided in Supplementary Data 6.

Functional annotation and enrichment analysis. The functional enrichment of sets of proteins with phosphopeptides most reduced in knockdown experiments at 29 h.p.i. and 37 h.p.i. was assessed using Ontologizer⁶⁴. Gene association files containing gene ontology (GO) terms for *P. falciparum*, *S. cerevisiae* and *Homo sapiens* were from <http://www.geneontology.org/gene-associations> (ref. 65; downloaded 21 May 2015). To generate comparative heatmaps of GO terms for both time points we selected the most specific terms, that is, those without children, which we refer to as 'tips' for convenience. Enrichment *P* values were included in the heatmap if they were present at either time point, and *P* values for non-tip terms were included if the term was a tip at the other time point. GO term annotations of the proteins detected in this study are provided in Supplementary Data 3 and defined in Supplementary Data 7.

Functional comparison of the PfCRK4-regulated set of phosphoproteins. The functional similarity between PfCRK4 and other protein kinases was assessed by comparing GO terms of the PfCRK4-regulated set with GO terms of reference kinase substrate sets. Reference human kinase substrate sets were obtained from PhosphoSitePlus (<http://www.phosphosite.org/staticDownloads.do>)²⁸ on 4 May 2015, and the substrate set for *S. cerevisiae* (Sc) cdc28 came from ref. 27. Reference kinases with fewer than 30 identified substrates were omitted from the analysis. Functional enrichment was assessed as described above. To calculate the relatedness of the substrate sets of kinases with PfCRK4, the number of terms in the intersect of the set of significantly enriched functions from the PfCRK4-regulated set and the substrate set from the reference kinases was divided by the number of significant functional terms in the substrate set from the reference kinase.

Identification and enrichment analysis of phosphorylation motifs. Alignments of phosphopeptides with reduced abundance in the absence of Shield-1 were manually inspected. The two motifs discernable in this set may be retrieved from tab-delimited tables of triskaidekapeptides by the regular expressions⁶⁶ $\{[A-Z]\{6\}\{[ST]\}[IVLFMWA].[RKH]\}$ (the S ϕ xK motif; ϕ , hydrophobic amino acid; x, any amino acid) and $\{[A-Z]\{6\}\{[ST]P\}$ (the S/TP motif). The set of phosphopeptides detected in this study (Supplementary Data 4) was searched with these regular expressions, and the percentage of peptides composed of these motifs was calculated. Phosphopeptides containing S ϕ xK and S/TP motifs are listed in Supplementary Data 4. Sequence logos were made from alignments of phosphopeptides containing S ϕ xK and S/TP motifs from sets of phosphopeptides reduced in the absence of Shield-1 using Weblogo (<http://weblogo.berkeley.edu>)⁶⁷.

Data availability. The data supporting the results of this study are available within the paper and its Supplementary Information and Supplementary Data. Sequences of oligonucleotides and plasmids generated for this study are available from the corresponding author upon request.

Received 29 May 2016; accepted 13 January 2017;
published 17 February 2017; corrected 6 March 2017

References

1. Francia, M. E. & Stripen, B. Cell division in apicomplexan parasites. *Nat. Rev. Microbiol.* **12**, 125–136 (2014).
2. Read, M., Sherwin, T., Holloway, S. P., Gull, K. & Hyde, J. E. Microtubular organization visualized by immunofluorescence microscopy during erythrocytic schizogony in *Plasmodium falciparum* and investigation of post-translational modifications of parasite tubulin. *Parasitology* **106**, 223–232 (1993).
3. Arnot, D. E., Ronander, E. & Bengtsson, D. C. The progression of the intra-erythrocytic cell cycle of *Plasmodium falciparum* and the role of the centriolar plaques in asynchronous mitotic division during schizogony. *Int. J. Parasitol.* **41**, 71–80 (2011).
4. Farrell, J. A. & O'Farrell, P. H. From egg to gastrula: how the cell cycle is remodeled during the *Drosophila* mid-blastula transition. *Annu. Rev. Genet.* **48**, 269–294 (2014).
5. Tewari, R. *et al.* The systematic functional analysis of *Plasmodium* protein kinases identifies essential regulators of mosquito transmission. *Cell Host Microbe* **8**, 377–387 (2010).
6. Solyakov, L. *et al.* Global kinomic and phospho-proteomic analyses of the human malaria parasite *Plasmodium falciparum*. *Nat. Commun.* **2**, 565 (2011).
7. Dvorin, J. D. *et al.* A plant-like kinase in *Plasmodium falciparum* regulates parasite egress from erythrocytes. *Science* **328**, 910–912 (2010).
8. Farrell, A. *et al.* A DOC2 protein identified by mutational profiling is essential for apicomplexan parasite exocytosis. *Science* **335**, 218–221 (2012).
9. Paul, A. S. *et al.* Parasite calcineurin regulates host cell recognition and attachment by apicomplexans. *Cell Host Microbe* **18**, 49–60 (2015).
10. Armstrong, C. M. & Goldberg, D. E. An FKBP destabilization domain modulates protein levels in *Plasmodium falciparum*. *Nat. Methods* **4**, 1007–1009 (2007).
11. Chu, B. W., Banaszynski, L. A., Chen, L.-C. & Wandless, T. J. Recent progress with FKBP-derived destabilizing domains. *Bioorg. Med. Chem. Lett.* **18**, 5941–5944 (2008).
12. Taylor, H. M. *et al.* The malaria parasite cyclic GMP-dependent protein kinase plays a central role in blood-stage schizogony. *Eukaryotic Cell* **9**, 37–45 (2010).
13. Collins, C. R. *et al.* Malaria parasite cGMP-dependent protein kinase regulates blood stage merozoite secretory organelle discharge and egress. *PLoS Pathog.* **9**, e1003344 (2013).
14. Muralidharan, V., Oksman, A., Pal, P., Lindquist, S. & Goldberg, D. E. *Plasmodium falciparum* heat shock protein 110 stabilizes the asparagine repeat-rich parasite proteome during malarial fevers. *Nat. Commun.* **3**, 1310 (2012).
15. Beck, J. R., Muralidharan, V., Oksman, A. & Goldberg, D. E. PTEX component HSP101 mediates export of diverse malaria effectors into host erythrocytes. *Nature* **511**, 592–595 (2014).
16. Buchholz, K. *et al.* A high-throughput screen targeting malaria transmission stages opens new avenues for drug development. *J. Infect. Dis.* **203**, 1445–1453 (2011).
17. Doerig, C., Endicott, J. & Chakrabarti, D. Cyclin-dependent kinase homologues of *Plasmodium falciparum*. *Int. J. Parasitol.* **32**, 1575–1585 (2002).
18. Ward, P., Equinet, L., Packer, J. & Doerig, C. Protein kinases of the human malaria parasite *Plasmodium falciparum*: the kinome of a divergent eukaryote. *BMC Genomics* **5**, 79 (2004).
19. Coudreuse, D. & Nurse, P. Driving the cell cycle with a minimal CDK control network. *Nature* **468**, 1074–1079 (2010).
20. Hydring, P., Malumbres, M. & Sicinski, P. Non-canonical functions of cell cycle cyclins and cyclin-dependent kinases. *Nat. Rev. Mol. Cell Biol.* **17**, 280–292 (2016).
21. Aikawa, M., Huff, C. G. & Sprinz, H. Fine structure of the asexual stages of *Plasmodium elongatum*. *J. Cell Biol.* **34**, 229–249 (1967).
22. Russo, I., Oksman, A., Vaupel, B. & Goldberg, D. E. A calpain unique to alveolates is essential in *Plasmodium falciparum* and its knockdown reveals an involvement in pre-S-phase development. *Proc. Natl Acad. Sci. USA* **106**, 1554–1559 (2009).
23. Theron, M., Hesketh, R. L., Subramanian, S. & Rayner, J. C. An adaptable two-color flow cytometric assay to quantitate the invasion of erythrocytes by *Plasmodium falciparum* parasites. *Cytometry A* **77**, 1067–1074 (2010).
24. Songyang, Z. *et al.* Use of an oriented peptide library to determine the optimal substrates of protein kinases. *Curr. Biol.* **4**, 973–982 (1994).
25. Lowe, E. D. *et al.* Specificity determinants of recruitment peptides bound to phospho-CDK2/cyclin A. *Biochemistry* **41**, 15625–15634 (2002).
26. Yeeles, J. T. P., Deegan, T. D., Janska, A., Early, A. & Diffley, J. F. X. Regulated eukaryotic DNA replication origin firing with purified proteins. *Nature* **519**, 431–435 (2015).
27. Ubersax, J. A. *et al.* Targets of the cyclin-dependent kinase Cdk1. *Nature* **425**, 859–864 (2003).
28. Hornbeck, P. V. *et al.* Phosphositeplus, 2014: mutations, PTMs and recalibrations. *Nucleic Acids Res.* **43**, D512–D520 (2015).
29. Bozdech, Z. *et al.* The transcriptome of the intraerythrocytic developmental cycle of *Plasmodium falciparum*. *PLoS Biol.* **1**, e5 (2003).
30. Roques, M. *et al.* Plasmodium P-Type cyclin CYC3 modulates endomitotic growth during oocyst development in mosquitoes. *PLoS Pathog.* **11**, e1005273 (2015).
31. Trager, W. & Jensen, J. B. Human malaria parasites in continuous culture. *Science* **193**, 673–675 (1976).
32. Fidock, D. A. & Wellem, T. E. Transformation with human dihydrofolate reductase renders malaria parasites insensitive to WR99210 but does not affect the intrinsic activity of proguanil. *Proc. Natl Acad. Sci. USA* **94**, 10931–10936 (1997).
33. Boyle, M. J. M. *et al.* Isolation of viable *Plasmodium falciparum* merozoites to define erythrocyte invasion events and advance vaccine and drug development. *Proc. Natl Acad. Sci. USA* **107**, 14378–14383 (2010).
34. Schneider, C. A., Rasband, W. S. & Eliceiri, K. W. NIH image to ImageJ: 25 years of image analysis. *Nat. Methods* **9**, 671–675 (2012).
35. Johnson, J. D. *et al.* Assessment and continued validation of the malaria SYBR green I-based fluorescence assay for use in malaria drug screening. *Antimicrob. Agents Chemother.* **51**, 1926–1933 (2007).
36. Neuhauser, C. *Calculus For Biology and Medicine: Pearson New International Edition* (Pearson, 2013).
37. Tonkin, C. J. *et al.* Localization of organellar proteins in *Plasmodium falciparum* using a novel set of transfection vectors and a new immunofluorescence fixation method. *Mol. Biochem. Parasitol.* **137**, 13–21 (2004).
38. Dinglasan, R. R. *et al.* *Plasmodium falciparum* ookinetes require mosquito midgut chondroitin sulfate proteoglycans for cell invasion. *Proc. Natl Acad. Sci. USA* **104**, 15882–15887 (2007).

39. Flueck, C. *et al.* A major role for the *Plasmodium falciparum* ApiAP2 protein PfSIP2 in chromosome end biology. *PLoS Pathog.* **6**, e1000784 (2010).
40. Gallagher, J. R., Matthews, K. A. & Prigge, S. T. *Plasmodium falciparum* apicoplast transit peptides are unstructured *in vitro* and during apicoplast import. *Traffic* **12**, 1124–1138 (2011).
41. Billker, O. *et al.* Identification of xanthurenic acid as the putative inducer of malaria development in the mosquito. *Nature* **392**, 289–292 (1998).
42. Thathy, V. *et al.* Levels of circumsporozoite protein in the *Plasmodium* oocyst determine sporozoite morphology. *EMBO J.* **21**, 1586–1596 (2002).
43. Pasini, E. M., van den Ierssel, D., Vial, H. J. & Kocken, C. H. M. A novel live-dead staining methodology to study malaria parasite viability. *Malar. J.* **12**, 190 (2013).
44. Coppens, I. & Joiner, K. A. Host but not parasite cholesterol controls toxoplasma cell entry by modulating organelle discharge. *Mol. Biol. Cell* **14**, 3804–3820 (2003).
45. Villén, J. & Gygi, S. P. The SCX/IMAC enrichment approach for global phosphorylation analysis by mass spectrometry. *Nat. Protoc.* **3**, 1630–1638 (2008).
46. Paulo, J. A. *et al.* Effects of MEK inhibitors GSK1120212 and PD0325901 *in vivo* using 10-plex quantitative proteomics and phosphoproteomics. *Proteomics* **15**, 462–473 (2014).
47. Wessel, D. & Flügel, U. I. A method for the quantitative recovery of protein in dilute solution in the presence of detergents and lipids. *Anal. Biochem.* **138**, 141–143 (1984).
48. Paulo, J. A. & Gygi, S. P. A comprehensive proteomic and phosphoproteomic analysis of yeast deletion mutants of 14-3-3 orthologs and associated effects of rapamycin. *Proteomics* **15**, 474–486 (2015).
49. Kettenbach, A. N. & Gerber, S. A. Rapid and reproducible single-stage phosphopeptide enrichment of complex peptide mixtures: application to general and phosphotyrosine-specific phosphoproteomics experiments. *Anal. Chem.* **83**, 7635–7644 (2011).
50. Paulo, J. A., Gaun, A. & Gygi, S. P. Global analysis of protein expression and phosphorylation levels in nicotine-treated pancreatic stellate cells. *J. Proteome Res.* **14**, 4246–4256 (2015).
51. McAlister, G. C. *et al.* Increasing the multiplexing capacity of TMTs using reporter ion isotopologues with isobaric masses. *Anal. Chem.* **84**, 7469–7478 (2012).
52. Huttlin, E. L. *et al.* A tissue-specific atlas of mouse protein phosphorylation and expression. *Cell* **143**, 1174–1189 (2010).
53. Beausoleil, S. A., Villén, J., Gerber, S. A., Rush, J. & Gygi, S. P. A probability-based approach for high-throughput protein phosphorylation analysis and site localization. *Nat. Biotechnol.* **24**, 1285–1292 (2006).
54. Elias, J. E. & Gygi, S. P. Target-decoy search strategy for increased confidence in large-scale protein identifications by mass spectrometry. *Nat. Methods* **4**, 207–214 (2007).
55. Elias, J. E. & Gygi, S. P. Target-decoy search strategy for mass spectrometry-based proteomics. *Methods Mol. Biol.* **604**, 55–71 (2010).
56. Edgar, R. C. MUSCLE: multiple sequence alignment with high accuracy and high throughput. *Nucleic Acids Res.* **32**, 1792–1797 (2004).
57. Stamatakis, A. RAxML version 8: a tool for phylogenetic analysis and post-analysis of large phylogenies. **30**, 1312–1313 (2014).
58. Finn, R. D. *et al.* Pfam: the protein families database. *Nucleic Acids Res.* **42**, D222–D230 (2014).
59. Finn, R. D. *et al.* HMMER web server: 2015 update. *Nucleic Acids Res.* **43**, W30–W38 (2015).
60. Webb, B. & Sali, A. Comparative protein structure modeling using MODELLER. *Curr. Protoc. Bioinformatics* **47**, 5–32 (2014).
61. Pettersen, E. F. *et al.* UCSF Chimera—a visualization system for exploratory research and analysis. *J. Comput. Chem.* **25**, 1605–1612 (2004).
62. Hartigan, J. A. Clustering. *Annu. Rev. Biophys. Bioeng.* **2**, 81–101 (1973).
63. Fischer, S. *et al.* Using OrthoMCL to assign proteins to OrthoMCL-DB groups or to cluster proteomes into new ortholog groups. *Curr. Protoc. Bioinformatics* **35**, 6.12.1–6.12.19 (2011).
64. Bauer, S., Grossmann, S., Vingron, M. & Robinson, P. N. Ontologizer 2.0—a multifunctional tool for GO term enrichment analysis and data exploration. **24**, 1650–1651 (2008).
65. Gene Ontology Consortium. Gene Ontology Consortium: going forward. *Nucleic Acids Res.* **43**, D1049–D1056 (2015).
66. Friedl, J. E. F. *Mastering Regular Expressions* (O'Reilly Media, 2006).
67. Crooks, G. E., Hon, G., Chandonia, J.-M. & Brenner, S. E. Weblogo: a sequence logo generator. *Genome Res.* **14**, 1188–1190 (2004).

Acknowledgements

The authors thank the members of the Duraisingh Laboratory for discussions and critical reading of the manuscript, D.F. Wirth for continuous guidance and support and S.T. Prigge, P. Sinnis, M.T. Makler and J. C. Rayner for sharing reagents. The authors acknowledge the Microscopy Facility at the Johns Hopkins School of Medicine. The authors thank H. Hurd and P. Eggleston for the *An. gambiae* KEELE strain. This work was supported by the National Institutes of Health (NIH R21 1R21AIO88314-01A1 to M.T.D.), a Wellcome Trust Project grant (094752/Z/10/Z to D.A.B. and M.T.D.), a Deutsche Forschungsgemeinschaft research fellowship (GA 1668/2-1 to M.G.), a Pediatric Scientist Development Program Fellowship award (K12-HD000850 to J.D.D.), an NIH/NIDDK grant (K01 DK098285 to J.A.P.), an HFSP award (RGY0073/2012 to J.G.K. and R.R.D.), the Bloomberg Family Foundation through the Johns Hopkins Malaria Research Institute, the NIH National Center for Research Resources (UL1 RR 025005), the Malaria Research Institute of The Johns Hopkins Bloomberg School of Public Health (R.R.D.).

Author contributions

M.G. designed, performed and interpreted much of the experimental work. J.M.G. analysed the phosphoproteomic data and provided bioinformatics support. J.D.D., J.A.P., J.G.K., A.K.T., A.S.P. and I.C. designed and performed specific experimental work. J.Y. constructed plasmids. R.H.Y.J. provided bioinformatics support. B.E. performed western blots. D.A.B., R.R.D. and S.P.G. provided reagents and intellectual input into study design. M.G., J.D.D. and M.T.D. conceived the study. M.G., J.M.G. and M.T.D. wrote the manuscript. All authors commented on the manuscript.

Additional information

Supplementary information is available for this paper.

Reprints and permissions information is available at www.nature.com/reprints.

Correspondence and requests for materials should be addressed to M.T.D.

How to cite this article: Ganter, M. *et al.* *Plasmodium falciparum* CRK4 directs continuous rounds of DNA replication during schizogony. *Nat. Microbiol.* **2**, 17017 (2017).

Competing interests

The authors declare no competing financial interests.

Erratum: *Plasmodium falciparum* CRK4 directs continuous rounds of DNA replication during schizogony

Markus Ganter, Jonathan M. Goldberg, Jeffrey D. Dvorin, Joao A. Paulo, Jonas G. King, Abhai K. Tripathi, Aditya S. Paul, Jing Yang, Isabelle Coppens, Rays H. Y. Jiang, Brendan Elsworth, David A. Baker, Rhoel R. Dinglasan, Steven P. Gygi and Manoj T. Duraisingh

Nature Microbiology **2**, 17017 (2017); published online 17 February 2017; corrected 6 March 2017.

In the version of this Letter originally published, the in-text citations to Supplementary Table 1 and Supplementary Data 1–7 were ambiguous. This has now been corrected in all versions of the Letter so that there is a clear distinction between the different files, with citations to Supplementary Table 1 and Supplementary Data 1–7 now appearing in the text. In addition, the definition of DIC in Fig. 2 was placed incorrectly. This has now been moved to Fig. 2b, in keeping with the figure panels.